

AperTO - Archivio Istituzionale Open Access dell'Università di Torino

## Lung imaging during acute respiratory distress syndrome : CT- and PET-scanning

**This is a pre print version of the following article:**

*Original Citation:*

*Availability:*

This version is available <http://hdl.handle.net/2318/1613579> since 2016-11-30T20:35:33Z

*Published version:*

DOI:10.1016/j.tacc.2011.05.006


*Terms of use:*

Open Access

Anyone can freely access the full text of works made available as "Open Access". Works made available under a Creative Commons license can be used according to the terms and conditions of said license. Use of all other works requires consent of the right holder (author or publisher) if not exempted from copyright protection by the applicable law.

(Article begins on next page)

**AUTHOR QUERY FORM**

|   |   |   |
|---|---|---|
| <br>ELSEVIER | <b>Journal:</b> TACC<br><br><b>Article Number:</b> 35 | <b>Please e-mail or fax your responses and any corrections to:</b><br><br><b>E-mail:</b> <a href="mailto:corrections.eseo@elsevier.tnq.co.in">corrections.eseo@elsevier.tnq.co.in</a><br><br><b>Fax:</b> +31 2048 52789 |
|---|---|---|

Dear Author,

Please check your proof carefully and mark all corrections at the appropriate place in the proof (e.g., by using on-screen annotation in the PDF file) or compile them in a separate list. To ensure fast publication of your paper please return your corrections within 48 hours.

For correction or revision of any artwork, please consult <http://www.elsevier.com/artworkinstructions>.

Any queries or remarks that have arisen during the processing of your manuscript are listed below and highlighted by flags in the proof.

| <b>Location<br/>in article</b> | <b>Query / Remark: Click on the Q link to find the query's location in text<br/>Please insert your reply or correction at the corresponding line in the proof</b> |
|--------------------------------|---|
| <b>Q1</b>                      | Please check and approve the insertion of the Figure citations (1,2) in the text. Correct if necessary.   |

Thank you for your assistance.



Contents lists available at ScienceDirect

## Trends in Anaesthesia and Critical Care

journal homepage: [www.elsevier.com/locate/tacc](http://www.elsevier.com/locate/tacc)

## REVIEW

## Lung imaging during acute respiratory distress syndrome: CT- and PET-scanning

Giacomo Bellani<sup>a</sup>, Pietro Caironi<sup>b,\*</sup><sup>a</sup> Dipartimento di Medicina Sperimentale, Università degli Studi di Milano-Bicocca, Dipartimento di Medicina Perioperatoria e Terapie Intensive, Azienda Ospedaliera San Gerardo, Monza, Italy<sup>b</sup> Dipartimento di Anestesiologia, Terapia Intensiva e Scienza Dermatologiche, Fondazione IRCCS Ca' Granda – Ospedale Maggiore Policlinico, Università degli Studi di Milano, Via F. Sforza 35, 20122 Milano, Italy

## S U M M A R Y

## Keywords:

Computed tomography

X-ray

Positron-emission tomography

Respiratory distress syndrome

Adult

In this article we review some of the main findings obtained by Computed Tomography (CT) and Positron Emission Tomography (PET) concerning the pathophysiology of Acute Respiratory Distress Syndrome (ARDS). CT is based on the detection of physical densities, allowing measurement of regional aeration. Beginning from the revolutionary concept of the “baby lung”, CT findings later led to a further evolution of the ARDS lung model, showing that the lungs behave as a wet “sponge”, with the dependent regions collapsing under the superimposed weight. More recently, CT scan has been used to quantify the potential for lung recruitment, showing that this is extremely heterogeneous among ARDS patient and tightly linked to mortality. PET (possibly combined with CT) is a functional imaging technique, based on the detection of a labeled molecule administered to a subject. Based on which molecule is used, different functions can be imaged. In the course of experimental ARDS injection of [<sup>13</sup>N]N<sub>2</sub>– labeled saline has been used to image regional gas exchange. Administration of [<sup>18</sup>F]FDG allows the image of cellular metabolic activity, reflecting neutrophils activation during inflammation. This technique has been applied in experimental ARDS and, more recently, in patients showing, for example, that inflammatory activity of the lungs is markedly increased also in “normally aerated” regions and, in some cases, even higher than in the non-aerated ones. We will present here some of the findings obtained by the two techniques in the clinical setting of ARDS, also discussing some of their possible future applications.

© 2011 Elsevier Ltd. All rights reserved.

## 1. Introduction

In Medicine, the application of imaging techniques has always been considered crucial for its growth, as it is well documented in the last century of its history, when the first “medical” X-ray has been performed by Wilhelm Röntgen, on December 22, 1895. The application of Computed Tomography (CT) and, more recently, of Positron Emission Tomography (PET) to the study of Acute Lung Injury and Acute Respiratory Distress Syndrome (ALI/ARDS) may be another great example of the crucial role of imaging techniques, as applied to Intensive Care Medicine. In fact, when the first CT-scan images have been performed in patients affected by ARDS in 1986,<sup>1,2</sup> it immediately appeared clear how its introduction in the study of this syndrome might have led to a complete revolution of its pathophysiological understanding and clinical treatment. Similarly, the introduction of PET-scanning in investigating vascular, permeability, lung perfusion and lung inflammation, performed by different groups in the last 10 years,<sup>3–5</sup> has begun an analogous “new era”, allowing the possibility of “making visible” and

therefore “measurable” specific processes undergoing the development and the characterization of ALI/ARDS. In the current review we will briefly overview the rationale underlying the application of both CT and PET-scanning in patients affected by ARDS, summarizing firstly the physical principles of the two techniques, and secondly highlighting the procedures undergoing their quantitative analysis. Moreover, we will present some of the findings obtained with their application in the clinical setting of ALI/ARDS. Finally, we will briefly discuss some of the possible future application of the two techniques (Fig. 1).

## 2. CT-scanning: principles and rationale of analysis

## 2.1. Physical principles

The theoretical approach allowing the use of CT-scan images for a quantitative analysis of the lung parenchyma relies on the numerical values associated to each unit in which the images are divided (i.e., the voxels), and which are defined as CT numbers.<sup>6</sup> Indeed, this value represents the linear attenuation coefficient ( $\mu$ ) of X-ray beams through the matter, in other words, the reduction of the radiation

\* Corresponding author. Tel.: +39 (0)2 5503 3232; fax: +39 (0)2 5503 3230.

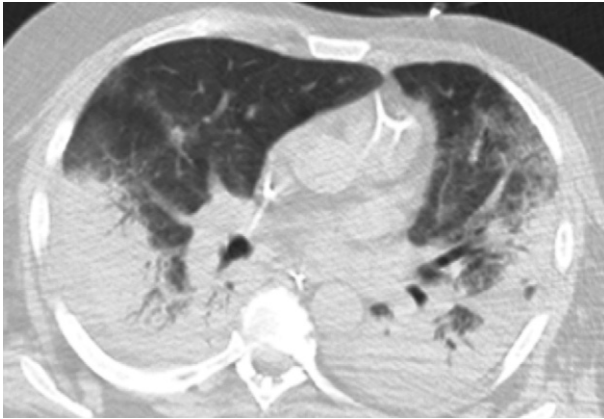


**Fig. 1.** Representative CT-scan image of a patients affected by acute respiratory distress syndrome (ARDS) obtained at the lung base. As shown, lung parenchyma is mainly characterized by a relative healthy region in the non-dependent (para-sternal in supine position) regions, while in contrast it is mainly characterized by atelectasis and/or consolidation in the dependent lung regions (para-vertebral in supine position).

intensity after the passage through the matter, as referred to the linear attenuation coefficient of water (a material of reference):

$$CT = 1000 \times \left( \frac{\mu_{\text{material}} - \mu_{\text{water}}}{\mu_{\text{water}}} \right)$$

where  $\mu_{\text{material}}$  denotes the linear attenuation coefficient of the material analyzed, and  $\mu_{\text{water}}$  denotes the linear attenuation coefficient of water. In order to magnify the small differences of linear attenuation coefficients of different materials, a factor scale of 1000 is employed.<sup>7</sup> The extreme importance and usefulness of CT numbers relies on their strict association with the physical density of the material the X-ray beam has passed through, as previously demonstrated in an experimental setting.<sup>6,8</sup> The “CT number” or “the CT physical density” is measured in Hounsfield Units (HU), ranging from +1000 HU, which approximates the physical density of bone (complete absorption), and –1000 HU, which approximates the physical density of air (complete transparency). Zero HU approximately equals the physical density of water. The lung tissue, which includes different anatomical entities (such as cells, extravascular fluid, blood, and others<sup>7</sup>), has a physical density very close to that of water (1 g/ml or 0 HU). Consequently, the range of density we have to consider when dealing with the lung parenchyma is included between 0 HU and –1000 HU. If we consider the lung parenchyma as a mixture of air and tissue (including cells, blood, extravascular fluid, etc.), a voxel with a CT number of –700 HU will be characterized by a 70% of air, and a 30% of lung tissue.<sup>9</sup> In summary, the gas volume of a specific lung region of interest (ROI) may be computed as follows:

$$\text{Gas volume}_{\text{ROI}} = \text{Total volume}_{\text{ROI}} \times \left( \frac{\text{mean } CT_{\text{ROI}}}{-1000} \right)$$

where the  $\text{Total volume}_{\text{ROI}}$  denotes the total volume of the specific lung area, and  $\text{mean } CT_{\text{ROI}}$  denotes the mean density, expressed as CT number, of the specific lung area. On the other hand, the amount of tissue included in a specific lung area may be computed as follows:

$$\text{Tissue weight}_{\text{ROI}} = \text{Total volume}_{\text{ROI}} \times \left[ 1 - \left( \frac{\text{mean } CT_{\text{ROI}}}{-1000} \right) \right]$$

where  $\text{Total volume}_{\text{ROI}}$  denotes the total volume of the specific lung area, and  $\text{mean } CT_{\text{ROI}}$  denotes the mean density, expressed as CT number, of the specific lung area (Fig. 2).

## 2.2. Lung compartments

To further investigate the morphology of the lung parenchyma, especially in a diseased lung, it may be more convenient to divide the lung parenchyma in different compartments according to their degree of aeration.<sup>9</sup> Based upon the frequency distribution of the CT numbers of an entire slice of lung CT-scan, four different compartments can be recognized: 1 – a non-aerated compartment (CT number between –100 HU and 0 HU), which represents the portion of lung parenchyma which is gas-less, i.e. collapse, consolidated, or filled with extravascular fluid; 2 – a poorly-aerated compartment (CT number between –101 HU and –500 HU); 3 – a normally aerated compartment (CT number between –501 HU and –900 HU), which represent the major compartment in healthy lung; 4 – a hyperinflated compartment (CT number between –901 HU and –1000 HU<sup>9</sup>).

## 3. CT scan and theoretical modeling of ALI/ARDS lung

### 3.1. The “baby lung” model

After the first identification of ARDS by Asbaugh and colleagues,<sup>10</sup> the lung parenchyma affected by this syndrome has been traditionally considered as “stiff”, based upon the extremely low compliance of the respiratory system consistently observed. The first CT-scan performed on a patient affected by ARDS revealed a quite different picture on an axial lung image: rather than homogeneous, the disease appeared to have a quite uneven distribution.<sup>1</sup> Three different zones, in fact, could be recognized: a near-normal area in the non-dependent lung regions, a ground-glass opacification in the middle lung regions, and a consolidated area in the most dependent lung regions. A subsequent quantitative analysis of CT-scan images revealed that the near-normal areas localized in the non-dependent lung regions is truly normally aerated lung tissue, but the quantity of this lung compartment is extremely reduced (about 200–300 g) as compared to that of a normal subject (about 700 g). This observation led to the concept of the “baby lung”: rather than “stiff”, the lung affected by ARDS is small, with a normal portion having the dimension of the lung of a 5–6 years-old child.<sup>9</sup> These findings gradually changed our view of ARDS and in particular our view about how to ventilate ARDS patients. In fact, given the functional morphology of ARDS lung as observed, it becomes quite evident that the application of very high tidal volume to a very small lung will inevitably generate extremely high lung stress and strain that may lead to tissue rupture (i.e. barotraumas), and/or to lung remodeling.<sup>11</sup> Thus, the premises for a more “gentle” ventilatory treatment of the lung were in front of every physician.

### 3.2. The “sponge lung” model

Initially, the “baby lung” was thought to be an anatomical entity, usually located in the non-dependent lung regions. As a consequence, this conceptual framework was the theoretical base for the proposal of prone positioning in ARDS patients.<sup>12</sup> In fact, it was hypothesized that by turning the patient in prone position, the “baby lung”, once located in the dependent lung regions after the change in position, would have received more blood perfusion according to a gravity-dependent pattern.<sup>13</sup> Surprisingly, while systemic oxygenation did actually improve in most of the patients, we consistently observed a redistribution of the lung densities, from the most dependent lung regions (the para-vertebral areas in supine position), to the most dependent lung regions in prone position (the para-sternal lung areas<sup>13,14</sup>). From the subsequent regional analysis of CT-scan images it appeared that pulmonary



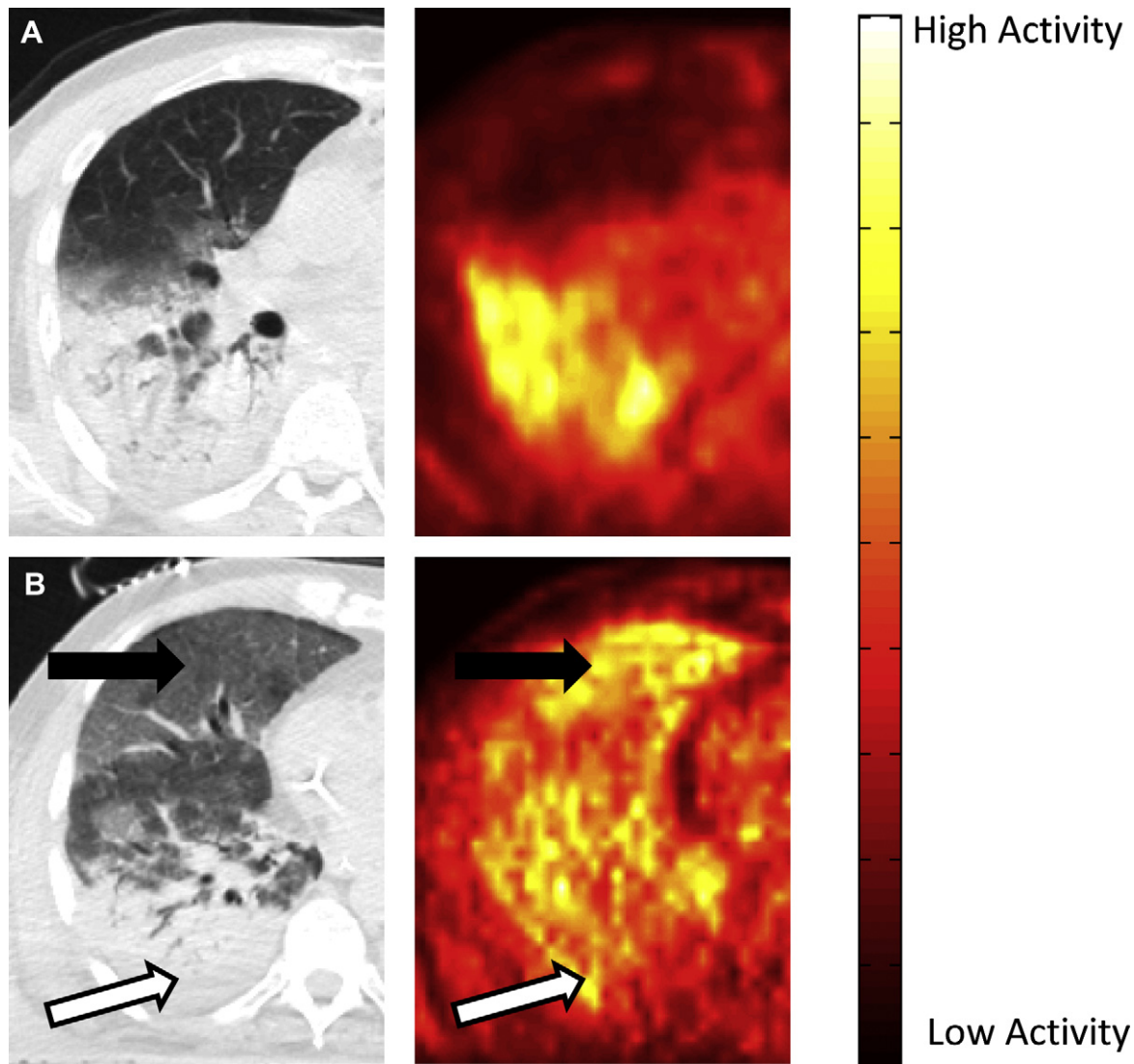


**Fig. 2.** Representative images of cross-registered CT (acquired at mean airway pressure) and  $[^{18}\text{F}]\text{FDG}$  PET from two patients with ARDS. PET images represent the average pulmonary  $[^{18}\text{F}]\text{FDG}$  concentration over the last 20 min of acquisition. *Panel A:* In this patient the distribution of  $[^{18}\text{F}]\text{FDG}$  parallels that of the opacities detected on CT, being higher in the non-dependent regions with less aeration. *Panel B:* In this patient the pattern is reverse being the  $^{18}\text{F}\text{FDG}$  uptake more intense in the “poorly” and “normally” aerated regions (black arrow), in comparison with the dorsal, “non-aerated” areas (white arrow).

edema accumulates within the lung parenchyma according to an evenly pattern along the sterno-vertebral gradient, and it's not distributed according to gravitational forces,<sup>15</sup> as previously observed both in experimental and clinical settings.<sup>16</sup> A novel model of ARDS pathophysiology was therefore proposed, i.e. the “sponge lung”<sup>17</sup>: lung edema formation affects the whole lung in an evenly distribution, but, based upon the increased lung weight, in the presence of gravitational forces, the increased mass will tend to generate lung collapse in the most dependent lung regions, where the excess tissue weight will be greater. As a consequence, the increased lung weight, while collapsing the most dependent lung regions, will squeeze out the gas from the most dependent to the non-dependent lung regions, leading to the classical appearance of lung parenchyma on CT-scan images.

### 3.3. The “recruitable lung” and the “consolidated lung” model

Although the importance of lung recruitment has been commonly well accepted in the clinical treatment of ARDS

patients,<sup>18</sup> the mechanisms underlying its pathophysiology have not yet completely understood. In order to better elucidate this aspect, we recently investigated the maximal potential for lung recruitment, as detected by CT-scan, in a large population affected by ALI/ARDS.<sup>19</sup> The first interesting finding observed was a largely variation of the potential for lung recruitment among the study population: the maximal lung recruitability varied from a quite negligible fraction to more than 50 percent of the total lung weight. Surprisingly, independently of the potential for lung recruitment, the amount of the consolidated lung tissue, i.e., the amount of gas-less tissue non openable even applying 45 cmH<sub>2</sub>O airway pressure, was quite constant throughout the population, corresponding to about 24 percent of the total lung tissue weight. It followed that the maximal lung recruitability appeared to be strictly associated to the total amount of non-aerated lung tissue at baseline, i.e. the gas-less tissue. Thus, based upon these observations, a novel model of ARDS lung was proposed. When the initial insult leading to ARDS affect the lung parenchyma, the extent of the inflammatory reaction will influence the development of lung edema, and therefore the

development of gravity-dependent alveolar collapse (i.e., the potential for lung recruitment). It is thus conceivable that the constant extent of the consolidated lung tissue reflects the “core disease” of ARDS, whereas the associated collapsed and therefore recruitable lung tissue reflects the extent of the surrounding inflammatory reaction, which will vary among different patients, and that will be associated with the gravity of the disease and therefore with the final outcome.<sup>19,20</sup>

### 3.4. The importance of intra-tidal lung opening and closing

The theoretical development of different models of ARDS lung has subsequently founded the bases for different approach to the setting of positive end-expiratory pressure (PEEP) during mechanical ventilation of ALI/ARDS patients. In particular, after the wide use of pressure-volume curve and the lower inflection point,<sup>21</sup> the introduction of the “sponge” model,<sup>17</sup> together with the concept of the “open-lung approach”,<sup>22</sup> has progressively led investigators to the application of relatively high levels of PEEP, aimed at counterbalancing the increased weight of ARDS lung tissue, thereby contrasting the development of lung collapse. Nonetheless, although tremendous efforts have been made to demonstrate the beneficial effects of high levels of PEEP in ALI/ARDS patients, three different large multicenter randomized clinical trials have concluded towards no difference in outcome for patients randomized to receive either a lower or a higher level of PEEP.<sup>23–25</sup>

Although the solution of such crucial question is still debate,<sup>26</sup> we think that the main reason for the neutral effects of high PEEP levels in such studies may be found in the absence of a characterization of patients randomized to the two arms with regard to their lung recruitability. In our study, in fact, we have observed that the amount of lung tissue recruited during the increase of PEEP applied is strictly associated to the total amount of potential for lung recruitment: the higher is the maximal lung recruitability, the greater is the amount of collapsed lung tissue recruited during the increase of PEEP from 5 to 15 cmH<sub>2</sub>O.<sup>19</sup> Moreover, in a subsequent analysis of the same investigation, we have recently observed that the application of high levels of PEEP may dramatically reduced the amount of lung tissue undergoing cycling opening and closing (i.e., one of the main determinant of the ventilator-associated lung injury) only in patients with a higher potential for lung recruitment, where the effects of such application appeared to favor the reduction of opening and closing lung tissue as compared to the associated increase in lung strain.<sup>27</sup> To further confirm these findings and the potential mechanism by which PEEP may improve outcome, the amount of opening and closing lung tissue has also appeared to be an independent risk factor for mortality. Thus, the rationale for the potential beneficial effects of the application of high level of PEEP has been fully elucidated, being strictly associated to the total extent of the potentially recruitable lung.

### 4. CT-scanning and ARDS definition

During the past years, it has been progressively recognized that, irrespective of the initial insult, ARDS is constantly characterized by an alteration of the permeability of the alveolar-capillary membrane, with the formation of high-permeability lung edema. Nonetheless, this alteration has never been directly included in the definition of ARDS. Among several available ARDS definition, the most widely accepted is the one proposed by the American-European Consensus Conference which relies primarily on hypoxemia (PaO<sub>2</sub>/FiO<sub>2</sub> lower than 300) and the presence of bilateral infiltrates, as detected on chest X-ray, in the absence of left atrial hypertension.<sup>28</sup> All the definitions of ARDS available at the moment

include the presence of bilateral pulmonary infiltrates, as detected by chest X-ray, which is considered a surrogate of the presence of high-permeability lung edema. Unfortunately, the chest X-ray “infiltrates” may be the morphological sign of different conditions, such as lung atelectasis, consolidation, interstitial edema, intra-alveolar flooding or consolidation, etc.<sup>7</sup> In contrast, CT-scanning may be a much better tool to detected lung edema formation, especially by applying to CT-images a quantitative analysis, thereby looking at the excess tissue mass.<sup>29</sup>

In the investigation mentioned above,<sup>19</sup> which included patients affected by ALI or ARDS according to the American-European Consensus Conference, we also examined, as control groups, patients affected by unilateral pneumonia and patients with healthy lungs, undergoing whole lung CT scanning for diagnostic purposes. By looking at the total lung tissue weight, which approximates the weight of the “healthy” lung tissue plus the excess tissue mass due to edema accumulation, we observed that patients with ALI/ARDS had significantly greater lung tissue weight (about 1500 g) than patients with either healthy lungs or unilateral pneumonia (respectively about 850 and 1200 g). However, when dividing the overall ALI/ARDS population according to the potential for lung recruitment, we observed that the difference in lung tissue weight between ALI/ARDS patients and patients with healthy lung was mainly due to the ALI/ARDS patients with a higher potential for lung recruitment (about 1700 g), being the lung tissue weight of ALI/ARDS patients with a lower potential for lung recruitment very similar to that observed in patients with unilateral pneumonia (about 1250 g). These findings highlight the importance of considering the real pathognomonic lesion, and therefore the hallmark sign, of ARDS, i.e. high-permeability lung edema, in its definition, as previously suggested.<sup>30</sup> In fact, it is surprising that in about half of the patients currently considered as affected by ALI/ARDS, as defined by the American-European Consensus Conference, the amount of collapsed lung tissue, which is strictly related to the formation of gravity-dependent lung edema, is almost negligible, and, even more, very similar to that observed in patients with unilateral pneumonia, which, by definition, are not included into the ALI/ARDS definition.

### 5. PET-scanning: methodology

Positron Emission Tomography is a functional imaging technique based on the detection of photons generated by the annihilation of a positron emitted by an instable isotope labeling a compound administered to a subject.<sup>31</sup> PET is nowadays mostly used for neoplasm staging and follow-up, but, depending on the tracer used, it potentially allows the in-vivo imaging of several functions; for this reason PET has been applied, mainly for research purposes, to a large number of different diseases both in the clinical and pre-clinical setting; in the field of intensive care medicine most of the focus has been put on acute lung injury (ALI) and acute respiratory distress syndrome (ARDS).

A PET scanner is basically constituted by a number of adjacent rings of detectors. The imaging procedure requires the administration of a biologically active molecule substituted in one atom with an unstable isotope, which emits one positron (anti-particle of an electron). This, in turn, annihilates with one electron, yielding two photons, travelling in two opposite directions. When two photons are detected within a narrow delay by two detectors, an “event” is recorded. After an adequate acquisition period, it is possible, in analogy to a computed tomography (CT) acquisition, to reconstruct the spatial and temporal distribution of the tracer. However, the feature unique to PET does not reside much in the acquisition equipment, but in the tracers employed (commonly 11-carbon, 13-nitrogen, 15-oxygen and 18-fluoride, used as a substitute

for hydrogen allowing to label hundreds of organic molecules without altering biological properties<sup>31</sup> and to image virtually any physiological process that can be individuated by following the spatial and temporal kinetic of this molecule. We will now focus some of the results obtained by PET more relevant to the ALI/ARDS patients.

## 6. PET-scanning and gas exchange

Lungs' ability to perform gas exchange depends on regional aeration, perfusion and by the optimal regional matching of these. Each one of this function can be imaged, separately, by PET. For example, following inhalation of a steady state concentration of nitrogen, (which has an extremely low solubility, with a partition coefficient  $\lambda_{\text{water/air}}$  of 0.015), the regional activity will be proportional to the gas content of that region and, once the subject starts to breath fresh gases, it is possible to measure regional ventilation as a function of nitrogen washout.<sup>32</sup> Moreover labeled nitrogen can be delivered to the subject after having been dissolved in saline solution, by intravenous injection. Later on the technique was reappraised at Massachusetts General Hospital in Boston by Dr. Venegas and his group who developed the single bolus technique.<sup>33</sup> With this approach, applicable both to human and animal studies, a single bolus of saline solution with [<sup>13</sup>N]N<sub>2</sub> gas dissolved is infused intravenously during 30–60 s apnea. When the tracer reaches the alveoli, the nitrogen evolves from the blood to the gaseous phase accumulating proportionally to the regional perfusion. In the case of blood perfusing non-aerated units (shunt), the regional activity, after a peak will decrease, as tracer is moved towards the pulmonary veins and left atrium. Again, during ventilation, the nitrogen washout will be proportional to the regional specific ventilation. This technique has the advantage of providing, in addition to the quantitative measurements of  $V_a/Q$  ratios, a topographical distribution of perfusion, ventilation and shunting blood flow. An indirect validation of the technique has been provided by Vidal Melo et al. who, gathering ventilation/perfusion images from different types of lung injury have been able to predict the arterial blood gases.<sup>34</sup>

Besides the study of asthmatic human subjects, this technique has been applied to experimental models of ALI. Musch et al. clarified that the mechanisms by which a recruitment maneuver can actually worsen gas exchange, is a shift in perfusion from aerated to non-aerated lung regions.<sup>35</sup> Moreover the data provided by PET aided to address the relationship between the impairments in lung aeration and gas exchange. The authors, in keeping with the literature, firstly evidenced the lack of a systematic relationship between lung's aeration (expressed as gas fraction) and shunt fraction at a global lung level. At the same time they showed that, at a regional level a tight linear relationship exists between aeration and shunting blood flow. Interestingly this relationship held true even if positive end-expiratory pressure (PEEP) was changed. This relationship was interpreted as suggesting a "quantal" loss of gas-exchanging units: in other words, below a certain threshold alveolar units do not loose uniformly aeration, rather some of them become atelectatic, while the remaining unit preserve aeration and gas exchange ability. The increase in regional shunt fraction could thus be due to an increase in the ratio of shunting to normally aerated alveoli. Finally, it is possible to predict global shunt fraction only if regional perfusion is taken into account, since each region contributes to global shunt fraction proportionally to its perfusion.<sup>36</sup> PET with [<sup>13</sup>N]N<sub>2</sub> has been used to study on gas exchange of several diseases (such as VILI, smoke inhalation, asthma, pulmonary embolism) and of several therapies (such as pulmonary vasodilators, prone position, recruitment maneuvers).<sup>37</sup> Other authors had used labeled water ([<sup>15</sup>O]H<sub>2</sub>O) to image lung perfusion

and extravascular water showing, for instance, a severe blunt of pulmonary hypoxic vasoconstriction during sepsis.<sup>38</sup>

## 7. PET-scanning and lung inflammation

[<sup>18</sup>F]fluoro-2-deoxy-D-glucose is an analog of glucose, which is uptaken by cells at the same rate of glucose; the molecule is phosphorylated as naïve glucose, but, due to the absence of one oxygen atom, it cannot be further processed and it is trapped into the cells. The intensity of the glycolytic metabolism of the cells is thus mirrored by the accumulation of <sup>18</sup>FDG. PET was originally devised for the study of the heavily glucose dependent brain metabolism, although the burst of PET into clinical practice has been allowed by the fact that [<sup>18</sup>F]FDG is actively uptaken by neoplastic cells from many different tumors. In order to quantify the uptake of [<sup>18</sup>F]FDG two kind of methods have been mainly used, so far. The first class, "semi-quantitative", routinely used in the clinical practice, relies on the use of the standardized uptake value (SUV), defined as the tissue concentration of tracer as measured by a PET scanner divided by the activity injected divided by body weight. Quantitative methods are based on the application of mathematical multi-compartmental models, fitted to the tracer time course. One of the most commonly used is the simplified Patlak's graphical analysis: the ratio of tissue to plasma activity is plotted as a function of the ratio of the integral of plasma activity normalized to plasma activity. The experimental points are fitted with a linear regression whose slope represents the net uptake of FDG (Ki) and the intercept represents the initial volume of distribution. It is important to underline that the models initially developed for the brain were subsequently transferred to the study of the lungs,<sup>39</sup> although this might be debatable, due to the important anatomical differences and more sophisticated models have been specifically developed for the lung.<sup>40</sup>

Increased [<sup>18</sup>F]FDG signal has been reported in the course of several experimental and clinical inflammatory processes in the lungs.<sup>41</sup> The uptake of [<sup>18</sup>F]FDG occurs primarily by activated neutrophils, whose metabolism (especially during the respiratory burst triggered by the rolling and adhesion phases) is heavily dependent on anaerobic glycolysis, requiring an elevated uptake of glucose. These data are supported by microautoradiographic studies showing after in vivo administration of [<sup>18</sup>F]FDG or ex-vivo incubation with 3HDG (deoxyglucose labeled with tritium) the source of radiation was localized in neutrophils,<sup>42</sup> also in case of numerical abundance of macrophages.<sup>43</sup> In keeping with this finding it has been shown that, in a model of ventilator induced lung injury (VILI) the depletion of neutrophils, without affecting other cellular types, causes, basically, a disappearance of the [<sup>18</sup>F]FDG signal.

Several experimental models of lung injury, such as the administration of streptococcus pneumonia,<sup>42</sup> oleic acid, endotoxin<sup>44</sup> and bleomycin, VILI and smoke inhalation have been studied by PET [<sup>18</sup>F]FDG. In a sheep model of VILI, in which one of the two lungs was injured by alveolar overexpansion (high peak inspiratory pressure) and collapse (negative end-expiratory pressure) the injured lung shows a marked increase of metabolic activity after only 90 min of injurious ventilation; at this time point, despite the injured lung had a marked loss of aeration, arterial hypoxemia was modest, probably as an effect of pulmonary hypoxic vasoconstriction diverting blood flow from the injured lung, as shown by the ventilation perfusion PET scan with injected [<sup>13</sup>N]N<sub>2</sub> (see above). PET with [<sup>18</sup>F]FDG has been used in humans to image lung metabolic activity (likely to reflect inflammation) in the course of several types of lung disease, including asthma,<sup>45</sup> COPD<sup>45</sup> infection<sup>46</sup> and rejection of lung's transplant. In all such conditions PET allowed the imaging of lung's inflammation. Among eight patients with risk



factors for ALI, 75% of those subsequently developing ALI had a “diffuse” uptake of [ $^{18}\text{F}$ ] FDG (i.e., both in non aerated and normally aerated regions on CT), while in all patients subsequently not developing ALI the uptake of [ $^{18}\text{F}$ ]FDG was confined to the regions of poor or absent aeration.<sup>47</sup> Bellani and coworkers have shown in ten mechanically ventilated patients with ALI/ARDS that the metabolic activity of the lungs was markedly increased in comparison with healthy controls, correlating with oxygenation impairment. The inflammation was spread also to the regions appearing “normally aerated” on CT scan; thus providing direct evidence that ALI/ARDS affects the whole lung, even the regions spared by aeration loss. Albeit the exact reasons have not been fully understood, two different pattern were observed in the regional association between metabolic activity and regional loss of aeration: in some patients the highest [ $^{18}\text{F}$ ]FDG uptake co-existed with aeration loss, decreasing in regions of restored aeration. On the contrary, in some patients the areas of normal or poor aeration bore metabolic activity similar to or greater than that of areas with aeration loss.<sup>5</sup>

The effect of mechanical ventilation on regional [ $^{18}\text{F}$ ]FDG uptake (likely, as stated, to reflect inflammation) was assessed in a cohort of mechanically ventilated ALI/ARDS patients, in whom, after the imaging with PET, two additional sets of CT scans were obtained, one at end-expiration and one at end-inspiration, thus allowing to image the regional deformations of lung parenchyma caused by tidal inflation. At variance with the extensive literature data suggesting that alveolar cyclic opening and closing represents a relevant source of injury and inflammation, no difference in metabolic activity was found between regions collapsed throughout the respiratory cycle and those undergoing intratidal recruitment–derecruitment, thus somehow challenging the actual relevance of this mechanisms in patients managed with low tidal volumes<sup>48</sup> and relatively high PEEP.<sup>49</sup> However, metabolic activity of the “normally aerated” tissue was correlated both with plateau pressure (with a steep increase above 26–27 cmH<sub>2</sub>O) and with the ratio between tidal volume and end-expiratory lung volume, the latter representing the space available for ventilation, over which tidal volume is distributed. Interestingly, these correlations held true (ore became even tighter) if the metabolic activity of normally aerated tissue was normalized by the activity of the non-aerated one, not exposed to the stress of ventilation, thus supporting a potential causative role of this factor in promoting the inflammation of normally aerated tissue.<sup>50</sup>

## 8. Further application of PET-scanning

Table 1 reports some of the tracers that have been described and used for studying lung function.

Given the number and the variety of tracers employed in PET scanning of the lung it would be impossible to synthesize in this review the whole body of obtained results. However, it is certainly

**Table 1**  
The table enlists the lung's functions which have been, so far, imaged by PET and the radioactive compounds used as respective tracers.

| Tracer                                       | Imaged Function   |
|--|---|
| [ $^{14}\text{C}$ ]CO                        | Regional blood volume   |
| [ $^{18}\text{F}$ ]Fluorocaptopril           | Pulmonary Angiotensin-converting Enzyme (ACE) expression, binding and inhibition                  |
| [ $^{13}\text{N}$ ]N <sub>2</sub> (injected) | Regional perfusion and gas exchange (i.e. regional ventilation shunting blood flow, gas trapping) |
| [ $^{13}\text{N}$ ]N <sub>2</sub> (inhaled)  | Regional aeration and ventilation   |
| [ $^{15}\text{O}$ ]H <sub>2</sub> O          | Regional perfusion and extravascular lung water   |
| $^{68}\text{Ga}$ -transferrin                | Endothelial permeability  |
| [ $^{11}\text{C}$ ]PK11195                   | Presence of macrophages (specifically binds benzodiazepine peripheral receptors)                  |

worth to recall the results obtained in a cornerstone study by Dr Schuster group's who demonstrated that, during ARDS, despite lung density had a pronounced vertical gradient (as opposed to control subjects), the lung permeability (measured by pulmonary transcapillary escape rate of  $^{68}\text{Ga}$ -transferrin) was abnormally high but evenly distributed along the vertical axis. This result gave a direct evidence that ARDS affects the entire lung, independently of the patchy distribution of aeration loss.<sup>51</sup>

## 9. Future directions

Imaging applications have certainly a number of limitations, since they are not bedside, but require patient's transportation (which can be a relevant drawback in critically ill patients), imply a given amount of radiation exposure, and they may require relatively high costs. With this regards, we think that a particular discussion is required for the potential radiation exposure, being an important limitation that has to be balanced against the potential advantages of a given radiological imaging procedure. Although epidemiological data linked the exposure to low-dose radiation and the development of neoplasms, and work exposure is strictly monitored and restricted, radiation exposure for patients is typically not recorded and its restriction is left to the physicians good clinical practice. The average dose received from a patients for a CT scan of the thorax is 7 mSv (increasing up to 15 mSv if an imaging protocol with medium contrast for the detection of pulmonary embolism is used) and that for a PET study is 14.1 mSv.<sup>52</sup> To allow comparisons it can be said that the annual dose from natural background is about 3 mSv, while annual exposures of 20–50 mSv and >50 mSv are considered to be high and very high respectively,<sup>53</sup> although an excess of cancers has not been observed either in animals or in humans for doses below 100 mSv.<sup>54</sup> It must be remembered that these values apply to the general population and in critically ill patients the appropriate indication to a radiological study is crucial for the benefits to outweigh the risks.

Besides such limitations, imaging techniques may bear a number of advantages, among which one of the mostly relevant is possibly the ability of detecting the whole range of heterogeneity characteristic of the diseased lung. CT has been in the field for decades and it is already commonly used for the management of patients with ALI/ARDS. Its capabilities in quantitating the amount of parenchyma available for recruitment or overinflated have clearly been demonstrated; a challenge for the future clinical research is probably to demonstrate that the use of these data for the management of the patients (for example in setting PEEP<sup>55</sup>) can actually lead to an improvement of the outcome. The use of PET is certainly less spread, but rapidly increasing; the availability of scanners in a growing number of institution will give to more and more researcher the opportunity to engage research with this tool. At the same time, taking advantage of the flexibility of the technique, the development of new tracers will broad the spectrum of addressable functional processes. So far, however, the greatest challenge for PET in the field of critical care medicine (in analogy to what has already happened for oncology) is to fill the gap from being an exquisite research tool to a clinical resource with an impact on patient's management.

## Conflict of interest

None.

## References

- Gattinoni L, Mascheroni D, Torresin A, Marcolin R, Fumagalli R, Vesconi S, et al. Morphological response to positive end expiratory pressure in acute respiratory failure. Computerized tomography study. *Intensive Care Med* 1986;**12**: 137–42.



2. Maunder RJ, Shuman WP, McHugh JW, Marglin SI, Butler J. Preservation of normal lung regions in the adult respiratory distress syndrome. Analysis by computed tomography. *JAMA* 1986;**255**:2463–5.
3. Mintun MA, Dennis DR, Welch MJ, Mathias CJ, Schuster DP. Measurements of pulmonary vascular permeability with PET and gallium-68 transferrin. *J Nucl Med* 1987;**28**:1704–16.
4. Musch G, Layfield JD, Harris RS, Melo MF, Winkler T, Callahan RJ, et al. Topographical distribution of pulmonary perfusion and ventilation, assessed by PET in supine and prone humans. *J Appl Physiol* 2002;**93**:1841–51.
5. Bellani G, Messa C, Guerra L, Spagnoli E, Foti G, Patroniti N, et al. Lungs of patients with acute respiratory distress syndrome show diffuse inflammation in normally aerated regions: a [<sup>18</sup>F]-fluoro-2-deoxy-D-glucose PET/CT study. *Crit Care Med* 2009;**37**:2216–22.
6. Mull RT. Mass estimates by computed tomography: physical density from CT numbers. *AJR Am J Roentgenol* 1984;**143**:1101–4.
7. Gattinoni L, Caironi P, Pelosi P, Goodman LR. What has computed tomography taught us about the acute respiratory distress syndrome? *Am J Respir Crit Care Med* 2001;**164**:1701–11.
8. Gattinoni L, Presenti A, Torresin A, Baglioni S, Rivolta M, Rossi F, et al. Adult respiratory distress syndrome profiles by computed tomography. *J Thorac Imaging* 1986;**1**:25–30.
9. Gattinoni L, Pesenti A, Avalli L, Rossi F, Bombino M. Pressure-volume curve of total respiratory system in acute respiratory failure. Computed tomographic scan study. *Am Rev Respir Dis* 1987;**136**:730–6.
10. Ashbaugh DG, Bigelow DB, Petty TL, Levine BE. Acute respiratory distress in adults. *Lancet* 1967;**2**:319–23.
11. Rocco PR, Dos SC, Pelosi P. Lung parenchyma remodeling in acute respiratory distress syndrome. *Minerva Anestesiol* 2009;**75**:730–40.
12. Pelosi P, Caironi P, Taccone P, Brazzi L. Pathophysiology of prone positioning in the healthy lung and in ALI/ARDS. *Minerva Anestesiol* 2001;**67**:238–47.
13. Langer M, Mascheroni D, Marcolin R, Gattinoni L. The prone position in ARDS patients. A clinical study. *Chest* 1988;**94**:103–7.
14. Gattinoni L, Pelosi P, Vitale G, Pesenti A, D'Andrea L, Mascheroni D. Body position changes redistribute lung computed-tomographic density in patients with acute respiratory failure. *Anesthesiology* 1991;**74**:15–23.
15. Pelosi P, D'Andrea L, Vitale G, Pesenti A, Gattinoni L. Vertical gradient of regional lung inflation in adult respiratory distress syndrome. *Am J Respir Crit Care Med* 1994;**149**:8–13.
16. Gattinoni L, Caironi P. Prone positioning: beyond physiology. *Anesthesiology* 2010;**113**:1262–4.
17. Bone RC. The ARDS lung. New insights from computed tomography. *JAMA* 1993;**269**:2134–5.
18. Caironi P, Gattinoni L. How to monitor lung recruitment in patients with acute lung injury. *Curr Opin Crit Care* 2007;**13**:338–43.
19. Gattinoni L, Caironi P, Cressoni M, Chiumello D, Ranieri M, Quintel M, et al. Lung recruitment in patients with the acute respiratory distress syndrome. *N Engl J Med* 2006;**354**:1775–86.
20. Cressoni M, Caironi P, Polli F, Carlesso E, Chiumello D, Cadringer P, et al. Anatomical and functional intrapulmonary shunt in acute respiratory distress syndrome. *Crit Care Med* 2008;**36**:669–75.
21. Gattinoni L, Eleonora C, Caironi P. Monitoring of pulmonary mechanics in acute respiratory distress syndrome to titrate therapy. *Curr Opin Crit Care* 2005;**11**:252–8.
22. Lachmann B. Open up the lung and keep the lung open. *Intensive Care Med* 1992;**18**:319–21.
23. Brower RG, Lanken PN, MacIntyre N, Matthay MA, Morris A, Ancukiewicz M, et al. Higher versus lower positive end-expiratory pressures in patients with the acute respiratory distress syndrome. *N Engl J Med* 2004;**351**:327–36.
24. Meade MO, Cook DJ, Guyatt GH, Slutsky AS, Arabi YM, Cooper DJ, et al. Ventilation strategy using low tidal volumes, recruitment maneuvers, and high positive end-expiratory pressure for acute lung injury and acute respiratory distress syndrome: a randomized controlled trial. *JAMA* 2008;**299**:637–45.
25. Mercat A, Richard JC, Vielle B, Jaber S, Osman D, Diehl JL, et al. Positive end-expiratory pressure setting in adults with acute lung injury and acute respiratory distress syndrome: a randomized controlled trial. *JAMA* 2008;**299**:646–55.
26. Gattinoni L, Caironi P. Refining ventilatory treatment for acute lung injury and acute respiratory distress syndrome. *JAMA* 2008;**299**:691–3.
27. Caironi P, Cressoni M, Chiumello D, Ranieri M, Quintel M, Russo SG, et al. Lung opening and closing during ventilation of acute respiratory distress syndrome. *Am J Respir Crit Care Med* 2010;**181**:578–86.
28. Bernard GR, Artigas A, Brigham KL, Carlet J, Falke K, Hudson L, et al. The American-European consensus conference on ARDS. Definitions, mechanisms, relevant outcomes, and clinical trial coordination. *Am J Respir Crit Care Med* 1994;**149**:818–24.
29. Gattinoni L, Pesenti A, Bombino M, Baglioni S, Rivolta M, Rossi F, et al. Relationships between lung computed tomographic density, gas exchange, and PEEP in acute respiratory failure. *Anesthesiology* 1988;**69**:824–32.
30. Schuster DP. Identifying patients with ARDS: time for a different approach. *Intensive Care Med* 1997;**23**:1197–203.
31. Harris RS, Schuster DP. Visualizing lung function with positron emission tomography. *J Appl Physiol* 2007;**102**:448–58.
32. Richard JC, Le BD, Costes N, Bregon F, Tourville C, Lavenne F, et al. Alveolar recruitment assessed by positron emission tomography during experimental acute lung injury. *Intensive Care Med* 2006;**32**:1889–94.
33. Galletti GG, Venegas JG. Tracer kinetic model of regional pulmonary function using positron emission tomography. *J Appl Physiol* 2002;**93**:1104–14.
34. Vidal Melo MF, Layfield D, Harris RS, O'Neill K, Musch G, Richter T, et al. Quantification of regional ventilation-perfusion ratios with PET. *J Nucl Med* 2003;**44**:1982–91.
35. Musch G, Harris RS, Vidal Melo MF, O'Neill KR, Layfield JD, Winkler T, et al. Mechanism by which a sustained inflation can worsen oxygenation in acute lung injury. *Anesthesiology* 2004;**100**:323–30.
36. Musch G, Bellani G, Vidal Melo MF, Harris RS, Winkler T, Schroeder T, et al. Relation between shunt, aeration, and perfusion in experimental acute lung injury. *Am J Respir Crit Care Med* 2008;**177**:292–300.
37. Musch G, Venegas JG. Positron emission tomography imaging of regional lung function. *Minerva Anestesiol* 2006;**72**:363–7.
38. Schuster DP, Anderson C, Kozlowski J, Lange N. Regional pulmonary perfusion in patients with acute pulmonary edema. *J Nucl Med* 2002;**43**:863–70.
39. Schroeder T, Melo MF, Venegas JG. Analysis of 2-[Fluorine-18]-Fluoro-2-deoxy-D-glucose uptake kinetics in PET studies of pulmonary inflammation. *Acad Radiol* 2011;**18**:418–23.
40. Schroeder T, Vidal Melo MF, Musch G, Harris RS, Venegas JG, Winkler T. Modeling pulmonary kinetics of 2-deoxy-2-[<sup>18</sup>F]fluoro-D-glucose during acute lung injury. *Acad Radiol* 2008;**15**:763–75.
41. de PN, Tucci MR, Melo MF. Assessment of lung inflammation with <sup>18</sup>F-FDG PET during acute lung injury. *AJR Am J Roentgenol* 2010;**195**:292–300.
42. Jones HA, Clark RJ, Rhodes CG, Schofield JB, Krausz T, Haslett C. In vivo measurement of neutrophil activity in experimental lung inflammation. *Am J Respir Crit Care Med* 1994;**149**:1635–9.
43. Jones HA, Schofield JB, Krausz T, Boobis AR, Haslett C. Pulmonary fibrosis correlates with duration of tissue neutrophil activation. *Am J Respir Crit Care Med* 1998;**158**:620–8.
44. Zhou Z, Kozlowski J, Schuster DP. Physiologic, biochemical, and imaging characterization of acute lung injury in mice. *Am J Respir Crit Care Med* 2005;**172**:344–51.
45. Jones HA, Marino PS, Shakur BH, Morrell NW. In vivo assessment of lung inflammatory cell activity in patients with COPD and asthma. *Eur Respir J* 2003;**21**:567–73.
46. Jones HA, Sriskandan S, Peters AM, Pride NB, Krausz T, Boobis AR, et al. Dissociation of neutrophil emigration and metabolic activity in lobar pneumonia and bronchiectasis. *Eur Respir J* 1997;**10**:795–803.
47. Rodrigues RS, Miller PR, Bozza FA, Marchiori E, Zimmerman GA, Hoffman JM, et al. FDG-PET in patients at risk for acute respiratory distress syndrome: a preliminary report. *Intensive Care Med* 2008;**34**:2273–8.
48. Bruhn A, Bugedo D, Riquelme F, Varas J, Retamal J, Besa C, et al. Tidal volume is a major determinant of cyclic recruitment-derecruitment in acute respiratory distress syndrome. *Minerva Anestesiol* 2011;**77**:418–26.
49. Gattinoni L, D'Andrea L, Pelosi P, Vitale G, Pesenti A, Fumagalli R. Regional effects and mechanism of positive end-expiratory pressure in early adult respiratory distress syndrome. *JAMA* 1993;**269**:2122–7.
50. Bellani G, Guerra L, Musch G, Zanella A, Patroniti N, Mauri T, et al. Lung regional metabolic activity and gas volume changes induced by tidal ventilation in patients with acute lung injury. *Am J Respir Crit Care Med* 2011;**183**:1193–9.
51. Sandiford P, Province MA, Schuster DP. Distribution of regional density and vascular permeability in the adult respiratory distress syndrome. *Am J Respir Crit Care Med* 1995;**151**:737–42.
52. Mettler Jr FA, Huda W, Yoshizumi TT, Mahesh M. Effective doses in radiology and diagnostic nuclear medicine: a catalog. *Radiology* 2008;**248**:254–63.
53. Fazel R, Krumholz HM, Wang Y, Ross JS, Chen J, Ting HH, et al. Exposure to low-dose ionizing radiation from medical imaging procedures. *N Engl J Med* 2009;**361**:849–57.
54. Nagataki S. Computed tomography and radiation exposure. *N Engl J Med* 2008;**358**:850–1.
55. Sarge T, Talmor D. Targeting transpulmonary pressure to prevent ventilator induced lung injury. *Minerva Anestesiol* 2009;**75**:293–9.